20th AIAA Computational Fluid Dynamics Conference
27 - 30 June 2011, Honolulu, Hawaii

AIAA 2011-3589

Parallel Solution Adaptive Scheme for Three-Dimensional Turbulent Diffusion Flames with Detailed Tabulated Chemistry

Pradeep K. Jha * and Clinton P.T. Groth†

University of Toronto Institute for Aerospace Studies

4925 Dufferin Street, Toronto, Ontario, Canada, M3H5T6

Mathematical modelling of the effects of turbulence on detailed-chemistry is an important issue in the accurate and reliable numerical prediction of turbulent combustion processes. The highly non-linear nature of both turbulence and chemistry make this extremely challenging. In this study, a Presumed Conditional Moment (PCM) approach, based on a β probability density function (PDF), is combined with the Flame Prolongation of ILDM (FPI) tabulation method to model the effects of turbulence and detailed-chemistry for diffusion flames. The recently proposed FPI scheme incorporates the effects of the detailed-chemistry on the local flow field for laminar flames through the use of two independent scalars: mixture fraction and progress variable and their variances. The Favre-Averaged Navier-Stokes (FANS) equations, based on the two-equation k-ω turbulence model, are used herein to model the effects of the unresolved turbulence on the mean flow field. The governing partial-differential equations for mean quantities are solved using a parallel, Adaptive Mesh Refinement (AMR), fully-coupled finite-volume formulation on body-fitted, multi-block, hexahedral mesh for three-dimensional flow geometries. Two approaches for coupling the PCM-FPI approach with the parallel AMR finite-volume solution method are considered. The PCM-FPI results are compared to experimental data for both reacting and non-reacting flows associated with a Sydney bluff-body burner configuration. The computational cost of the PCM-FPI scheme is compared to the cost of the simplified Eddy Dissipation Model (EDM). A full description of the proposed numerical solution scheme for turbulent non-premixed flames is provided along with an evaluation and demonstration of its computational performance and predictive capabilities.

I. Introduction

Practical combustion processes involve thousands of intermediate species and reaction steps. An accurate representation of the flames in these cases will require tracking every species and reaction step involved in the combustion process which is practically impossible. Detailed-chemistry mechanisms have been proposed for certain common fuels which predict the flame properties quite well by tracking a finite number of species.[1–4] However, the numerical modelling of these detailed-chemistry schemes are still prohibitively expensive for relevant industrial applications.

A number of approaches have been proposed to reduce the size of combustion problems without compromising on the quality of results. The Intrinsic Low Dimensional Manifold (ILDM) proposed by Maas and Pope,[5] Systematic Reduction Method (SRM) as discussed by Peters,[6] Computational Singular Perturbation (CSP) by Lam and Goussis,[7] Piecewise Reusable Implementation of Solution Mapping (PRISM) by Tonse *et al.*,[8] Quasi-Steady-State-Assumption (QSSA) by Ren and Pope,[9] Reaction-Diffusion-Manifold (REDIM) by Bykov and Maas,[10] and Invariant Constrained Equilibrium Edge Pre-Image Curve (ICE-PIC) by Ren and Pope[11] are some approaches which try to reduce the size of the kinetic mechanisms for complex fuel oxidation and pollutant formation by systematically reducing the size of the detailed problem. This is done by identifying and eliminating unimportant reactions and species which do not have a significant effect on the final

*Ph.D. Candidate

†Professor

flame structure. All these above mentioned methods differ from each other mainly in how the unimportant species are determined and handled.

In the tabulation approaches, chemical structure of the flames are parametrized and expressed as a function of a reduced set of variables. Hence, just by knowing the values of these variables, the detailed structure of the flame can be predicted during the simulations. Some of the dimension reduction methods discussed above also adopt a tabulated data approach. Peters[12] has suggested the use of detailed chemistry solutions of one-dimensional counter-flow flames for a range varying strain rates as a means for describing the chemical kinetics of more complex diffusion flames. Furthermore, premixed flamelets have been used to tabulate chemistry in turbulent combustion modelling for both premixed and non-premixed flames.[13,14] The Flame Prolongation of ILDM (FPI)[15,16] and Flame Generated Manifold (FGM)[17] are two recently proposed approaches based on tabulation of premixed flamelets. Both of these approaches have been developed and applied successfully to different combustion regimes and are of considerable current interest as they are unifying methods that may be applied to both premixed and non-premixed flames.[16,18–21]

Probability density functions (PDF) are a popular tool to model the effect of turbulence on reactive flows. Bradley *et al.*[13,22] have shown that PDFs can be used with known laminar flamelet solutions to account for turbulence, and this model has been used in conjunction with Reynolds-averaged Navier-Stokes (RANS) models. A number of studies have validated the use of PDFs for turbulent reacting flows.[23–25] More recently, Vervisch *et al.*,[21] Domingo *et al.*[19,26] and others have adopted a presumed PDF approach, leading to presumed conditional moment (PCM) modelling, in conjunction with the FPI approach for dealing with turbulent chemistry. In this approach, the presumed PDFs of some scalars are used to derive the mean reaction rates and species concentrations. Richardson *et al.*[27] were the first to use a β-distribution as the presumed PDF. Some other distributions like the sinusoidal PDF, "clipped Gauss" distributions, and a triangular distribution have also been investigated by other researchers.[28–30] A comparison between the different presumed PDFs has been carried out by Jones[31] and Libby and Williams[32] who compare the numerical results with the experimental measurements of Kent and Bilger.[33] The results obtained showed that the double delta function is unsatisfactory and both the β and the clipped Gaussian PDFs give very similar agreement with experimental data. The FPI approach has been used with the presumed β-distribution in a number of studies, to model the turbulence-chemistry interaction for RANS-based models and large eddy simulations (LES) of turbulent flows.[19,21,26,34,35] Comparisons of the PCM-FPI method to other subfilter-scale methods for the LES of turbulent premixed flames have been carried out and reported in a recent study by Perez *et al.*[36]

Another interesting approach to reduce the computational costs is to use a solution-adaptive grid. The adaptive mesh refinement (AMR) algorithms developed for aerospace applications[37–44] are a promising way to generate solution-adaptive grids. Computational grids that automatically adapt to the solution of the governing equations are very effective in treating problems with disparate length scales, providing the required spatial resolution while minimizing memory and storage requirements. Recent progress in the development and application of AMR algorithms for reacting flows and premixed turbulent combustion is described by Bell *et al.*[45–47] and Gao and Groth.[48–50] Computational costs of reacting flow prediction can be further reduced by applying a domain decomposition procedure and solve the problem in a parallel fashion using multiple processors. Large massively parallel distributed-memory computers can provide many fold increases in processing power and memory resources beyond those of conventional single-processor computers and would therefore provide an obvious avenue for greatly reducing the time required to obtain numerical solutions of combusting flows.

While the potential of LES methods for turbulent reactive flows has certainly been demonstrated, RANS-based approaches are still used in the majority of practical engineering computations and will therefore be the focus here. This work seeks to combine the various numerical approaches described above for reducing the computational costs of predicting turbulent combusting flows, producing a parallel AMR method that uses the the PCM-FPI approach and finite-volume scheme for solving the Favre-Averaged Navier-Stokes (FANS) equations governing three-dimensional turbulent non-premixed reactive flows of compressible mixtures on body-fitted, multi-block, hexahedral mesh. A full discussion of the proposed solution technique is provided herein along with a demonstration of the computational performance and predictive capabilities of the proposed solution method.

II. Favre-Averaged Navier-Stokes Equations

In this study, the Favre-Averaged Navier-Stokes equations for a compressible thermally perfect gaseous mixture are used to describe turbulent non-premixed reactive flows. In this formulation, the continuity, momentum and energy equations for a N species mixture can be expressed using tensor notation as[51,52]

$$\frac{\partial \bar{\rho}}{\partial t} + \frac{\partial}{\partial x_i}\left(\bar{\rho}\widetilde{u_i}\right) = 0 \tag{1}$$

$$\frac{\partial}{\partial t}\left(\bar{\rho}\widetilde{u_i}\right) + \frac{\partial}{\partial x_i}\left(\bar{\rho}\widetilde{u_j}\widetilde{u_i}\right) = -\frac{\partial \bar{p}}{\partial x_i} + \frac{\partial}{\partial x_i}\left(\bar{\tau}_{ji} + \bar{\rho}\lambda_{ji}\right) \tag{2}$$

$$\frac{\partial}{\partial t}\left[\bar{\rho}\left(\widetilde{e} + \frac{\widetilde{u_i}\widetilde{u_i}}{2} + k\right)\right] + \frac{\partial}{\partial x_j}\left[\bar{\rho}\widetilde{u_j}\left(\widetilde{h} + \frac{\widetilde{u_i}\widetilde{u_i}}{2} + k\right)\right] = \frac{\partial}{\partial x_j}\left[\left(\frac{\mu}{\mathrm{Pr_L}} + \frac{\mu_t}{\mathrm{Pr_t}}\right)\frac{\partial \widetilde{h}}{\partial x_j} + \left(\mu + \sigma^*\frac{\bar{\rho}k}{\omega}\right)\frac{\partial k}{\partial x_j}\right] + \frac{\partial}{\partial x_j}\left[\widetilde{u_i}\left(\bar{\tau}_{ij} + \bar{\rho}\lambda_{ij}\right)\right] \tag{3}$$

where $\overline{w}$ is the time-averaged value of quantity w, $\widetilde{w}$ is the Favre-averaged value of quantity w, $\vec{x}$ is the position vector, ρ is the mixture density, $\vec{u}$ is the velocity vector, $p = \sum_{k=1}^{N} \rho Y_k R_k T$ is the pressure, $Y_k = m_k/m$ is the mass fraction of species k, m_k is the mass of species k present in the given volume, m is the total mass of gas in the volume, $\vec{g}$ is the body force vector, $\bar{\tau}_{ji}$ denotes the viscous stress tensor, λ_{ji} denotes the Reynolds stress tensor, e is the specific total energy, h is the internal energy $\sum_{k=1}^{N} Y_k h_k$, h_k is the absolute internal enthalpy for species k and, k is the turbulent kinetic energy, ω is the specific dissipation rate of the turbulent kinetic energy, $\mathrm{Pr_L}$ is the molecular Prandtl number and, $\mathrm{Pr_t}$ is the turbulent Prandtl number set to a constant value of 0.9. The viscous stress tensor is given by the constitutive relation

$$\bar{\tau}_{ij} = \mu\left(\frac{\partial \widetilde{u_i}}{\partial x_j} + \frac{\partial \widetilde{u_j}}{\partial x_i}\right) - \frac{2}{3}\delta_{ij}\frac{\partial \widetilde{u_k}}{\partial x_k} \tag{4}$$

where μ is the molecular viscosity and δ_{ij} is the Kroneckar delta function. The Boussinesq approximation is used to relate the Reynolds stress tensor, λ_{ij}, to the mean flow strain-rate tensor using a turbulent eddy viscosity, $\mu_t = \bar{\rho}k/\omega$, and is given by

$$\bar{\rho}\lambda_{ij} = \mu_t\left[\frac{\partial \widetilde{u_i}}{\partial x_j} + \frac{\partial \widetilde{u_j}}{\partial x_i} - \frac{2}{3}\delta_{ij}\frac{\partial \widetilde{u_k}}{\partial x_k}\right] - \frac{2}{3}\delta_{ij}\bar{\rho}k \tag{5}$$

The transport equation describing the time evolution of the mass fraction for the k^{th} species, Y_k, is given by

$$\frac{\partial}{\partial t}\left(\bar{\rho}\widetilde{Y_k}\right) + \frac{\partial}{\partial x_j}\left(\bar{\rho}\widetilde{u_j}\widetilde{Y_k}\right) = -\frac{\partial}{\partial x_j}\left[\left(\mathcal{D}^k + \mathcal{D}_t\right)\frac{\partial \widetilde{Y_k}}{\partial x_j}\right] + \bar{\dot{\omega}}_k \tag{6}$$

where $\mathcal{D}^k$ is the molecular diffusivity of species k and, $\mathcal{D}_t = \mu_t/\mathrm{Sc}_t$ is the turbulent diffusivity, Sc_t is the turbulent Schmidt number set to a constant value of 1.0 and, $\bar{\dot{\omega}}_k$ is the time-averaged mass reaction rate of species k produced by the chemical reactions.

The modified two-equation k-ω model of Wilcox[53] is used to model the unresolved turbulent flow quantities. Transport equations are solved for the turbulent kinetic energy, k, and the specific dissipation rate, ω, which are given by

$$\frac{\partial}{\partial t}\left(\bar{\rho}k\right) + \frac{\partial}{\partial x_j}\left(\bar{\rho}\widetilde{u_j}k\right) = \bar{\rho}\lambda_{ij}\frac{\partial \widetilde{u_i}}{\partial x_j} - \beta^*\bar{\rho}k\omega + \frac{\partial}{\partial x_j}\left[\left(\mu + \sigma^*\frac{\bar{\rho}k}{\omega}\right)\frac{\partial k}{\partial x_j}\right] \tag{7}$$

$$\frac{\partial}{\partial t}\left(\bar{\rho}\omega\right) + \frac{\partial}{\partial x_j}\left(\bar{\rho}\widetilde{u_j}\omega\right) = \alpha\frac{\omega}{k}\bar{\rho}\lambda_{ij}\frac{\partial \widetilde{u_i}}{\partial x_j} - \beta\bar{\rho}\omega^2 + \frac{\partial}{\partial x_j}\left[\left(\mu + \sigma\frac{\bar{\rho}k}{\omega}\right)\frac{\partial \omega}{\partial x_j}\right] \tag{8}$$

where σ^*, β^*, α, σ, and β are closure coefficients for the two-equation model. Thermodynamic and molecular transport properties of each gaseous species are prescribed herein using the empirical database compiled by Gordon and McBride.[54,55]

A. Near Wall Treatment of Turbulence

An automatic wall treatment method, which switches between the low-Reynolds-number formulation and the standard wall function depending on the mesh resolution, was used for near wall treatment of the k-ω turbulence model.[56] In the case of low-Reynolds-number formulation, it can be shown that

$$\lim_{y\to 0}\omega = \frac{6\nu}{\beta y^2} \tag{9}$$

where y is the normal distance from the wall. This expression is used to specify the value of ω directly for all values of $y^+ \leq 2.5$, where $y^+ = u_\tau y/\nu$ is the dimensionless distance from the wall, $u_\tau = \sqrt{\tau_w/\rho}$ is the friction velocity, and τ_w is the wall shear stress, provided there are 3-5 computational cells inside $y^+ = 2.5$. In the case of the wall function formulation, the expressions

$$k = \frac{{u_\tau}^2}{\sqrt{\beta_o^*}}, \qquad \omega = \frac{u_\tau}{\sqrt{\beta_o^*}\kappa y} \tag{10}$$

where κ is the Von Kármán constant $= 0.41$, are used to fully specify both k and ω for $y^+ \leq 30 - 250$. The automatic treatment switches between these two methods depending on mesh resolution using a blending function. In this procedure, k and ω are approximated by

$$k = \frac{u_\tau^2}{\beta_o^*}\frac{\min(y^+, 30)}{30}, \qquad \omega = \omega_o\sqrt{1 + \left(\frac{\omega_{wall}}{\omega_o}\right)^2} \tag{11}$$

where $\omega_o = \frac{6\nu}{\beta y^2}$ and $\omega_{wall} = \frac{u_\tau}{\sqrt{\beta_o^*}\kappa y}$. In the turbulent flow simulations discussed below, a relatively coarse mesh is used to start and automatic treatment is used only on the first cell off the wall. After obtaining an approximate solution on the coarse mesh and performing two or three levels of refinement such that there are at least 2-3 cells within the laminar sublayer, the low-Reynolds-number formulation is used for the solution.

III. Tabulated-Chemistry Approach

A. Mixture Fraction for Diffusion Flames

The mixture fraction, f, provides an indication of the fraction of local mass having its origin in the fuel stream of a non-premixed or diffusion flame. For a pure-mixing/non-reacting flow, the local value of any thermodynamic quantity, φ, can be expressed as a linear function of f using the relation

$$\varphi = \varphi_{F,0} f + \varphi_{O,0}(1 - f) \tag{12}$$

where $\varphi_{F,0}$ is the value of φ in the fuel stream and $\varphi_{O,0}$ represents the value of φ in the oxidizer stream. For a pure-mixing flow, one can arrive at the following relations between equivalence ratio, ϕ, and f

$$\phi(f) = s\frac{Y_{\mathrm{F}}}{Y_{\mathrm{O}}} = s\frac{Y_{\mathrm{F},0} f}{Y_{\mathrm{O},0}(1 - f)}, \tag{13}$$

$$f(\phi) = \frac{\phi}{\left(\phi + s\frac{Y_{\mathrm{F},0}}{Y_{\mathrm{O},0}}\right)} \tag{14}$$

where s is the stoichiometric oxygen-to-fuel mass ratio. Note that in a diffusion flame, the equivalence ratio corresponds to the equivalence ratio obtained when premixing the same mass of fuel and oxidizer streams. It does not correspond to the global equivalence ratio in the burner.

The mixture fraction can be expressed as a linear combination of the chemical elements involved in the flow. Using this definition, and summing all of the species transport equations for species k given by Equations (6), the final mixture fraction transport equation can be derived as

$$\frac{\partial}{\partial t}(\rho f) + \frac{\partial}{\partial x_i}(\rho u_i f) = \frac{\partial}{\partial x_i}\left(\rho \mathcal{D}_f \frac{\partial f}{\partial x_i}\right) \tag{15}$$

where $\mathcal{D}_f = \zeta/\rho C_p$ is the molecular diffusivity term of the mixture fraction, ζ is the thermal conductivity of the gas and, C_p is the gas specific heat at constant pressure.

Approach	Tabulated	Species PDEs Solved	Methodology
(1)	Y_i, $\dot{\omega}_{Y_c}$	No	Get Y_i from table using $Y_i = Y_i(f, Y_c)$. Use Y_i directly in the solver.
(2)	Y_i, $\dot{\omega}_{Y_c}$	Yes	Get Y_i from table. Reconstruct $\dot{\omega}_i$ using $\dot{\omega}_i \approx \dot{\omega}_{Y_c} \frac{\partial Y_i}{\partial Y_c}$. Use these $\dot{\omega}$ values in species PDEs.

Table 1: Different ways of coupling the FPI look-up table to the flow solver.

B. Flame Prolongation of ILDM (FPI)

FPI tabulation uses pre-computed one-dimensional laminar premixed flame solutions for calculating flame structures of more complex flames. The Cantera software package[57] is used to generate solutions for one-dimensional premixed flames using the detailed-chemistry GRI-Mech 3.0 mechanism.[1] In one-dimensional laminar premixed flame, all flame properties can be uniquely expressed as a function of the initial unburnt mixture being used, which is defined by the equivalence ratio of the mixture, ϕ, and the spatial coordinate direction, x, normal to the flame front, such that

$$\varphi = \varphi(\phi, x) \tag{16}$$

A new parameter called the progress of reaction variable, Y_c, is then introduced to remove the spatial coordinate in Equation (16). The FPI tabulation then takes the following form:

$$\varphi^{\mathrm{FPI}} = \varphi(\phi, x) = \varphi(f(\phi), Y_c(x)) \tag{17}$$

The progress of reaction Y_c evolves from zero to its equilibrium value, ${Y_c}^{\mathrm{Eq}}(f)$, along every mixture fraction surface. Vervisch *et al.*[21] propose the use of a normalized value of Y_c, called the progress variable, c, which is defined as

$$c = \frac{Y_c(f, x)}{{Y_c}^{\mathrm{Eq}}(f)} \tag{18}$$

The reason for using c over Y_c will be discussed in more detail in Section B. Hence, in the final FPI look-up table, all relevant thermodynamic quantities are expressed as a function of two variables

$$\varphi^{\mathrm{FPI}} = \varphi(f, c) \tag{19}$$

Fiorina *et al.*[58] suggest that a linear combination of the mass fraction of CO_2 and CO is a good choice for the progress of reaction variable for methane-air combustion, which is considered herein. As noted above, the FPI scheme requires the solution of a transport equation for the progress of reaction, Y_c, which can be written as

$$\frac{\partial}{\partial t}\left(\rho Y_c\right) + \frac{\partial}{\partial x_i}\left(\rho u_i Y_c\right) = \frac{\partial}{\partial x_i}\left(\rho \mathcal{D}_{Y_c} \frac{\partial Y_c}{\partial x_i}\right) + \rho \dot{\omega}_{Y_c} \tag{20}$$

where $\mathcal{D}_{Y_c} = \mu/\rho/\mathrm{Sc}_{Y_c}$ is the molecular diffusivity of Y_c, Sc_{Y_c} is the progress of reaction Schmidt number which is taken to have value of unity, and $\dot{\omega}_{Y_c}$ is the reaction rate of the progress of reaction variable which is pre-computed and stored in the look-up table during table-generation. A number of studies[16,19,58] have reported the validation of this tabulation method for laminar premixed flames.

In diffusion flames, the mixture fraction values can vary over the entire range from zero to one and so values outside the flammability limits of premixed flames may be encountered. To calculate the species mass fractions for points lying outside the range of valid premixed flame solutions, a linear interpolation is performed between the pure-mixing solution, given by Equation (12), and known solution for the rich/lean limit solution of the premixed laminar flame solution.[59] In addition, the reaction rates for the progress of reaction are set to zero outside the premixed flame flammability limits.

C. Coupling Tabulated Data with Flow Solver

The size of the FPI table is an important concern that can tax available computer memory when performing practical calculations, especially when dealing with non-premixed turbulent flames. Careful study shows that of the 53 GRI-Mech 3.0 species, only 7 species: CH_4, O_2, CO_2, CO, H_2O, H_2 and N_2 account for more than 99.5% of the total mass and energy of the mixture.[59,60] Therefore, only storing the information for these 7 species can give us a good indication of the flame structure and properties. To take into account the mass of the elements being carried by the remaining species, three additional species are also tabulated. Galpin *et al.*[60] has shown that H, OH and C_2H_2 make are a good choice as additional species for methane-air flames. Hence, the final look-up table stores data for 10 species. In the final look-up table, the mass fractions of the major species are used directly from the pre-computed solutions whereas the mass fractions of minor species, such as C_2H_2 and H_2, are calculated by ensuring atomic mass conservation.[61] For example, when the detail chemistry solution of all 53 species is known, the conservation of atomic mass of carbon atoms gives the following expression for calculating $Y_{C_2H_2}$ in the reduced set of species:

$$Y_{\mathrm{C_2H_2}} = \frac{\mathcal{M}_{\mathrm{C_2H_2}}}{n_{\mathrm{C_{C_2H_2}}}} \left(\sum_{j=1}^{N} Y_j \frac{n_{\mathrm{C}_j} \mathcal{A}_{\mathrm{C}}}{\mathcal{M}_j} - \sum_{\substack{j=1 \\ j \neq \mathrm{C_2H_2}}}^{M} Y_j \frac{n_{\mathrm{C}_j} \mathcal{A}_{\mathrm{C}}}{\mathcal{M}_j} \right) \tag{21}$$

where M is the number of species in the reduced set of FPI tabulation, n_{C_k} is the number of carbon atom in species k, $\mathcal{M}_k$ is the molecular weight of species k, and $\mathcal{A}_k$ is the atomic weight of element k.

Two approaches are considered here for coupling the FPI tabulated data to the flow solver.

- **Approach 1 – Tabulated Mass Fractions**: The look-up table stores the mass fractions of the reduced set of species. Individual species transport equations are not solved. Instead, local values of f and Y_c are used to obtain the species concentrations from the table using bi-linear interpolation.
- **Approach 2 – Tabulated Mass Fractions & Estimated Reaction Rates**: Highly diffusive species can have large gradient values. Resolving these high values using tabulated species mass fraction needs highly refined tables. Instead of using the mass-fractions from the look-up table, like in Approach 1, the species reaction rates are reconstructed using the following relation[26]

$$\dot{\omega}_i \approx \dot{\omega}_{Y_c} \frac{\partial Y_i}{\partial Y_c} \tag{22}$$

  The species mass balance equations are then solved directly using the above expression.

In both of the above approaches, the transport equations for mass, momentum, energy, are solved along with the equations for the mixture fraction and progress of reaction variable. Table 1 summarizes these approaches.

IV. Turbulence and FPI

A. Statistical Approach: Presumed Conditional Moment

The treatment of turbulence in the FPI methods is based on a stochastic approach where the reactive and diffusive properties of a flame are described using joint PDFs. To calculate the mean of a variable, φ, which is dependent on (say) N independent variables, $w_1, \ldots, w_N$, such that $\varphi = \varphi(w_1, \ldots, w_N)$, a joint PDF $P(w_1^*, \cdots, w_N^*; x, t)$ is introduced. The mean value of φ is then estimated as

$$\widetilde{\varphi}(x,t) = \int_{w_i} \cdots \int \varphi(w_1^*, \cdots, w_N^*) P(w_1^*, \cdots, w_N^*; x, t) dw_1^* \cdots dw_N^* \tag{23}$$

As shown earlier in Equation (19), in the FPI approach all thermochemical quantities, φ, are expressed as a function of two variables: the mixture fraction, f, and the progress variable, c. Hence, simplifying Equation (23) the mean value for FPI tabulated quantities can be expressed as

$$\widetilde{\varphi}(x,t) = \int_{f^*} \int_{c*} \varphi^{\mathrm{FPI}}(f^*, c^*) P(f^*, c^*) df^* dc^* \tag{24}$$

Using Bayes' theorem, the joint PDF of f and c in Equation (24) can be decomposed using the conditional PDF for c for a given value of f^*, $P(c^*|f^*)$, using the relation

$$P(f^*, c^*) = P(c^*|f^*)P(f^*) \tag{25}$$

However, DNS[19,21,62] and experimental results[63] suggest that in many cases $P(c^*|f^*)$ is weakly dependent on f^*. While this is true only for a proper selection of the progress of reaction variable, in the experimental set-up studied by Barlow *et al.*[63] for methane-air jet flames, it was observed that the conditional statistical behaviour of c constructed from a linear combination of CO and CO_2 weakly varies with mixture fraction. Hence,

$$P(f^*, c^*) = P(f^*)P(c^*) \tag{26}$$

It is important to note that the hypothesis of statistical independence with f applies to c only, which is a normalized quantity, but not to the progress of reaction Y_c or any other quantity φ extracted from the flamelet tables.[19,26] While this hypothesis of statistical independence is not strictly exact, it has been found to be a reasonable approximation for a appropriate choice of Y_c.[19] Substituting Equation (25) into Equation (24) and using Equation (26), the expression for the mean quantity, $\widetilde{\varphi}$, can be approximated by

$$\widetilde{\varphi}(x,t) = \widetilde{\varphi}^{\mathrm{PCM}}(x,t) = \int_{f^*}\int_{c*} \varphi^{\mathrm{FPI}}(f^*, c^*)P(f^*)P(c^*)df^*dc^* \tag{27}$$

The most convenient method for determining the PDFs $P(f^*)$ and $P(c^*)$ is to assume that the PDF can be prescribed by an n-parameter function and to relate the first n moments to these parameters. As the mixture fraction, f, is bounded between 0 and 1, the choice is reduced to a small number of physically realistic functions. In the present work, β-distributions are been used to described the PDFs of the both mixture fraction and progress variable. The β PDF is widely used in turbulent combustion modelling[21,60,62,64] and has a huge advantage in that it can be specified algebraically in terms of it's first two moments. A β-function is given by

$$P(Z^*) = \frac{(Z^*)^{(a-1)}(1-Z^*)^{(b-1)}}{\int_0^1 (Z^+)^{(a-1)}(1-Z^+)^{(b-1)}dZ^+} \tag{28}$$

The two parameters a and b defining β-PDF can be determined in terms of the mean and variance as

$$a = \widetilde{Z}\left(\frac{\widetilde{Z}(1-\widetilde{Z})}{Z_v^2} - 1\right) \quad , \qquad b = a\left(\frac{1}{\widetilde{Z}} - 1\right) \tag{29}$$

B. Tabulation for PCM-FPI

Within a turbulent flame, using Equation (18), the conditional mean of Y_c, $\widetilde{Y_c|f^*}$, for a given value of $f = f^*$ maybe written as

$$\widetilde{Y_c|f^*} = \widetilde{c|f^*}Y_c^{\mathrm{Eq}}(f^*) \tag{30}$$

Using the statistical independence argument, an approximation of the conditional mean can be expressed as

$$\widetilde{Y_c|f^*} \approx \widetilde{c}Y_c^{\mathrm{Eq}}(f^*) \tag{31}$$

Integrating Equation (31) over the mixture fraction surfaces with $P(f^*)$ leads to

$$\widetilde{Y}_c = \widetilde{c}\widetilde{Y_c^{\mathrm{Eq}}} \tag{32}$$

with

$$\widetilde{Y_c^{\mathrm{Eq}}} = \int_o^1 Y_c^{\mathrm{Eq}}(f^*)P(f^*)df^* \tag{33}$$

As discussed earlier, the mixture fraction PDF, $P(f^*)$, is presumed from its first and second moment. This requires solving for additional transport equations for the mean and variance of mixture fraction, $\widetilde{f}$ and f_v, respectively. Equation (15) can be used to arrive at the following transport equations for $\widetilde{f}$ and f_v:

$$\frac{\partial}{\partial t}\left(\overline{\rho}\widetilde{f}\right) + \frac{\partial}{\partial x_i}\left(\overline{\rho}\widetilde{u}_i\widetilde{f}\right) = -\frac{\partial \tau_f}{\partial x_i} + \frac{\partial}{\partial x_i}\left(\overline{\rho}\mathcal{D}_f\frac{\partial \widetilde{f}}{\partial x_i}\right) \tag{34}$$

$$\frac{\partial}{\partial t}\left(\overline{\rho}f_v\right) + \frac{\partial}{\partial x_i}\left(\overline{\rho}\widetilde{u}_i f_v\right) = \frac{\partial}{\partial x_i}\left(\overline{\rho}\mathcal{D}_f\frac{\partial f_v}{\partial x_i}\right) - \frac{\partial}{\partial x_i}\left(\tau_{f^2} - 2f\tau_f\right) + 2\overline{\rho}\mathcal{D}_f\frac{\partial f}{\partial x_i}\frac{\partial f}{\partial x_i} - 2\tau_f\frac{\partial f}{\partial x_i} - 2\overline{\rho}\chi_f \tag{35}$$

The unclosed turbulent fluxes are modelled using a gradient transport hypothesis such that

$$\tau_f = -\mathcal{D}_t \frac{\partial \widetilde{f}}{\partial x_i} \tag{36}$$

$$\left(\tau_{f^2} - 2f\tau_f\right) = -\mathcal{D}_t \frac{\partial f_v}{\partial x_i}, \tag{37}$$

The unknown source terms in Equation (35), the scalar dissipation rate of f, χ_f, is closed using a linear relaxation hypothesis

$$\chi_f = \mathcal{D}_t \frac{\partial \widetilde{f}}{\partial x_i} \frac{\partial \widetilde{f}}{\partial x_i} + C_f \omega f_v, \tag{38}$$

where C_f is the closure coefficient for f_v transport equation and is set to 1.0.

Equation (27) also requires knowledge of the PDF of c, $P(c^*)$, which is also assumed to be a β-PDF. This calls for the values of both the mean and variance of the progress variable, $\widetilde{c}$ and c_v, respectively. The value of $\widetilde{c}$ can be determined using Equation (32). Using the definition of variance, the variance c_v can be expressed as

$$c_v = \frac{Y_{cv}}{\widetilde{Y_c^{\mathrm{Eq}^2}}} + \widetilde{Y_c}^2 \left(\frac{1}{\widetilde{Y_c^{\mathrm{Eq}^2}}} - \frac{1}{\widetilde{Y_c^{\mathrm{Eq}}}^2} \right) \tag{39}$$

where, $\widetilde{Y_c^{\mathrm{Eq}^2}}$ is

$$\widetilde{Y_c^{\mathrm{Eq}^2}} = \int_o^1 Y_c^{\mathrm{Eq}^2}(f^*) P(f^*) df^* \tag{40}$$

Prescription of c and c_v requires values of $\widetilde{Y}_c$ and Y_{cv}, which are determined via solution of transport equations for these two quantities. The transport equation for these variables can be derived from Equation (20) and written as

$$\frac{\partial}{\partial t}\left(\overline{\rho}\widetilde{Y}_c\right) + \frac{\partial}{\partial x_i}\left(\overline{\rho}\widetilde{u}_i\widetilde{Y}_c\right) = -\frac{\partial}{\partial x_i}\left(\tau_{Y_c}\right) + \frac{\partial}{\partial x_i}\left(\overline{\rho}\mathcal{D}_{Y_c}\frac{\partial \widetilde{Y}_c}{\partial x_i}\right) + \overline{\rho}\widetilde{\dot{\omega}}_{Y_c} \tag{41}$$

$$\begin{aligned}\frac{\partial}{\partial t}\left(\overline{\rho}Y_{cv}\right) + \frac{\partial}{\partial x_i}\left(\overline{\rho}\widetilde{u}_i Y_{cv}\right) &= \frac{\partial}{\partial x_i}\left(\overline{\rho}\mathcal{D}_{Y_c}\frac{\partial \widetilde{Y}_c}{\partial x_i}\right) - \frac{\partial}{\partial x_i}\left(\tau_{Y_c{}^2} - 2Y_c\tau_{Y_c}\right) + 2\overline{\rho}\mathcal{D}_{Y_c}\frac{\partial \widetilde{Y}_c}{\partial x_i}\frac{\partial \widetilde{Y}_c}{\partial x_i} \\ &\quad -2\tau_{Y_c}\frac{\partial \widetilde{Y}_c}{\partial x_i} - 2\overline{\rho}\chi_{Y_c} + 2\overline{\rho}\left(\widetilde{Y_c\dot{\omega}_{Y_c}} - \widetilde{Y}_c\widetilde{\dot{\omega}}_{Y_c}\right)\end{aligned} \tag{42}$$

Here again, the unclosed turbulent flux is modelled using a gradient transport hypothesis in the same way as Equation (37) and the unclosed source term is modeled similar to Equation (38) with C_{Y_c} as the closure coefficient for Y_{cv} transport equation set to 1.0.

The unknown reaction rate terms that appear in Equation (41) and Equation (42) are also extracted from the look-up table during a turbulent reactive flow simulation. These values are also precomputed and stored in the look-up table at the time of table-generation using the following expressions

$$\widetilde{\dot{\omega}}_{Y_c} = \int_o^1 \int_o^1 \dot{\omega}_{Y_c}^{\mathrm{FPI}} P(c^*) P(f^*) dc^* df^* \tag{43}$$

$$\widetilde{Y_c\dot{\omega}_{Y_c}} = \int_o^1 \int_o^1 c^* Y_c^{\mathrm{Eq}}(f^*) \dot{\omega}_{Y_c}^{\mathrm{FPI}} P(c^*) P(f^*) dc^* df^* \tag{44}$$

The mean values of the mass fractions is calculated using the following relation

$$\widetilde{Y}_i = \int_o^1 \int_o^1 Y_i^{\mathrm{FPI}} P(c^*) P(f^*) dc^* df^* \tag{45}$$

For tabulation purposes, it is convenient if all the independent variables are normalized. In premixed flames, the maximum level of fluctuations of the progress variable is obtained when c is is fully segregated.[65] Under

these circumstances, c_v takes its maximum value $c_v = \widetilde{c}/(1-\widetilde{c})$. Using similar arguments for the mixture fraction, the variances of f and c are normalized using the following expressions

$$S_f = \frac{f_v}{\widetilde{f}(1-\widetilde{f})} \tag{46}$$

$$S_c = \frac{c_v}{\widetilde{c}(1-\widetilde{c})} \tag{47}$$

where S_f and S_c are are the the segregation factors of $\widetilde{f}$ and $\widetilde{c}$ respectively. Using these definitions, in the final look-up table for mean turbulent quantities, every thermochemical quantity is stored as

$$\widetilde{\varphi} = \varphi^{\mathrm{PCM}}(\widetilde{f}, S_f, \widetilde{c}, S_c) \tag{48}$$

Look-up tables for turbulent diffusion flames can become somewhat large and managing the size of the table is an important issue. In the present study for methane-air reacting flows, the dimensions of the table used were $(121 \times 20 \times 121 \times 20)$. The table was stored in a binary format and had a size of approximately 537 MB.

V. Eddy Dissipation Model (EDM)

In order to assess the performance of the PCM-FPI approach, numerical results obtained using this tabulation approach have been compared herein to similar results obtained using the so-called eddy-dissipation model (EDM) as proposed by Magnussen and Hjertager.[66] The EDM is a simplified model widely used in many practical and commercial combustion codes to handle the influence of turbulence-chemistry interactions in turbulent diffusion flames. It makes use of simple one-step global chemical kinetics and is based on the idea that the time scales associated with finite-rate chemistry are small compared to the fluid times scales and are not the rate determining factor in turbulent reactive flows. Due to their larger time scales, the turbulent motions effectively control the reaction rates. In this case, the mean reaction rate is controlled by the characteristic turbulent mixing time, ω. For simple one-step global reactions of fuel and oxidizer, the time-averaged reaction rate of the fuel, $\bar{\dot{\omega}}_F$, is then given by

$$\bar{\dot{\omega}}_F = C_{mag}\beta_o^*\omega \, \min(\widetilde{Y}_F, \widetilde{Y}_o/s) \tag{49}$$

where C_{mag} is the proportionality constant for EDM which is taken to be4.0 herein, $\widetilde{Y}_F$ is the mass fraction of the fuel, $\widetilde{Y}_O$ is the mass fraction of the oxidizer. For methane-air combustion of interest here, the one-step, five-species, chemical kinetic scheme as proposed by Westbrook and Dryer[67] is used, for which the global reaction is given by

$$\mathrm{CH_4} + 2\,\mathrm{O_2} \rightleftharpoons \mathrm{CO_2} + 2\,\mathrm{H_2O}$$

Given the EDM reaction rate for the fuel (methane), the reaction rates of all other species involved in the reaction above are calculated by using the stoichiometric coefficients of each species in the forward chemical reaction mechanism.

VI. Parallel AMR Finite-Volume Algorithm

A. Finite Volume Scheme

A finite volume scheme on a body-fitted multi-block hexahedral mesh is proposed to solve the system of partial-differential equations governing three-dimensional turbulent compressible flows for reactive thermally perfect gaseous mixtures. Applying the divergence theorem to the differential form of the system of governing equations in three-dimensional coordinates, one arrives at the following integral form

$$\frac{\mathrm{d}}{\mathrm{d}t}\int_V \mathbf{U}\mathrm{d}V + \oint_\Omega \vec{n}\cdot\vec{\mathbf{F}}\,\mathrm{d}\Omega = \int_V \mathbf{S}\mathrm{d}V \tag{50}$$

where $\mathbf{U}$ is the vector of conserved variables, $\vec{\mathbf{F}}$ the flux dyad consisting of both inviscid and viscous flux components,$\mathbf{S}$ is the source term, defined as $\mathbf{S} = \mathbf{S}_\mathrm{t} + \mathbf{S}_\mathrm{p} + \mathbf{S}_\mathrm{c}$, where $\mathbf{S}_\mathrm{t}$, $\mathbf{S}_\mathrm{p}$ and $\mathbf{S}_\mathrm{c}$ are the source terms

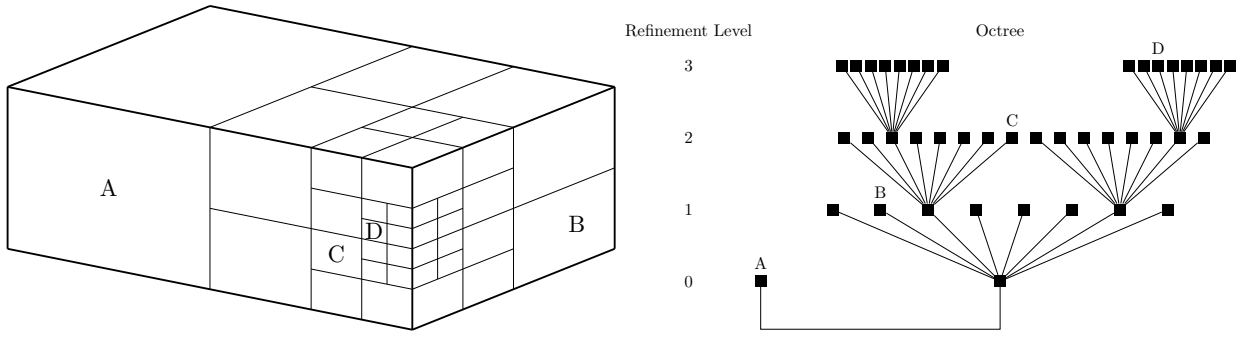

(a) Multi-block refinement

(b) Oct-tree structure for AMR scheme for three-dimensional geometry

Figure 1: Multi-block hexahedral AMR mesh showing solution blocks at various levels of refinement and the corresponding oct-tree data structure.

due to turbulence modelling, PCM-FPI scalar transport equations and finite rate chemistry respectively, V is the control volume, Ω is the surface area of the control volume and, $\vec{n}$ is the unit outward vector normal to the closed surface.

The inviscid (hyperbolic) component of the numerical flux at each cell face is evaluated using limited linear reconstruction[68] and the AUSM$^+$-up approximate Riemann solver proposed by Liou.[69] The viscous (elliptic) component of the numerical flux is evaluated by employing a diamond-path reconstruction procedure as described by Coirier and Powell.[70]

B. Block-Based Adaptive Mesh Refinement

Modelling practical combustion devices with complex chemistry, and turbulence quickly tax computational resources even on relatively coarse meshes. Unfortunately, high mesh densities are required in areas with steep gradients and small length scales to accurately capture these processes. These locations can change over time and would normally require the use of large, fine uniform meshes. A flexible block-based AMR scheme is adopted here to limit the number of necessary computational cells by dynamically adapting the mesh to meet solution requirements. Details of the scheme and its implementation in parallel are described by Gao *et al.*[49] In this approach, block-based domain decomposition is applied to a body-fitted hexahedral mesh. The grid blocks are organized in a hierarchical oct-tree data structure to facilitate automatic solution-directed mesh adaptation with physics-based criteria. The scheme borrows aspects from previous work by Berger and co-workers,[37,38,42,71] Quirk *et al.*,[39] and De Zeeuw *et al.*[40] for Cartesian grids and has similarities with the block-based approaches described by Quirk *et al.*[41] and Berger *et al.*[71] In the AMR scheme, the equations are first integrated forward in time on an initial structured, multi-block coarse mesh to obtain updated volume-averaged approximate solution quantities. The mesh is then adapted by coarsening or refining the blocks designated by the refinement criteria. A hierarchical tree-like data structure, shown in Figure 1b, is used to retain connectivity between solution blocks and track their refinement history. The blocks requiring refinement are termed "parents" and are divided into eight new blocks called "children". Each child is a new block with the same number of cells as its parent, doubling the mesh resolution in the region. Coarsening flagged blocks is carried out by reversing this process and combining eight children into one single parent.

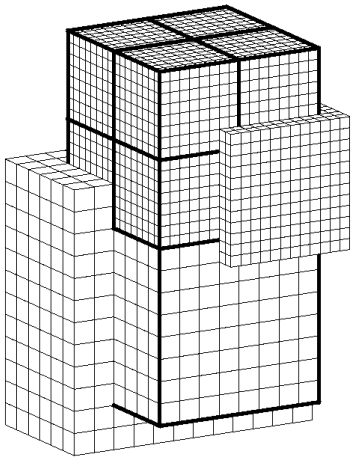

Figure 2: Sample multi-block grid and solution blocks depicting ghost cells.

For reacting flows, refinement is based on the gradients of both species mass fractions and temperature.

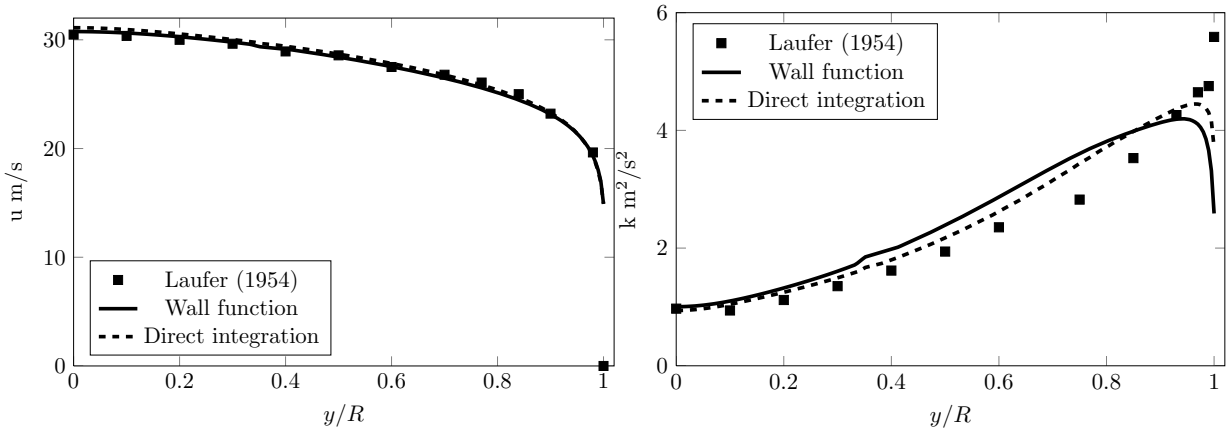

(a) Velocity profile

(b) Turbulent kinetic energy profile

Figure 3: Comparison of predicted solutions using a solver for 3D flows with experimental data for fully developed turbulent pipe flow, Re=50 000.

The refinement criteria employed here are defined by

$$\epsilon \propto |\vec{\nabla} T| \tag{51}$$

Based on either of this criteria, the mesh is refined and blocks are added wherever ϵ is large.

A measure of the efficiency of the block-based AMR scheme can be obtained by defining the refinement efficiency, η, as

$$\eta = 1 - \frac{N_{\text{cells}}}{N_{\text{uniform}}} \tag{52}$$

where N_{cells} is the total number of cells in the present grid and N_{uniform} is the total number of cells that would have been used on a uniform mesh composed of cells of the finest size on the current mesh. The efficiency of the AMR scheme improves as the number of refinement levels increase.

To further decrease the overall computational time, integration of the governing equations is performed in parallel. This is carried out by distributing the computational blocks among the available processors and simultaneously computing the solutions for each block on each processor. An even distribution of solution blocks is generally sought on homogeneous architectures while a weighted distribution is permissible for computations performed on heterogeneous systems such as networked workstations or computational grids. To ensure efficient load balancing, blocks are organized using a Morton ordering space filling curve which co-locates nearest neighbors on the same processor.[42] This minimizes the amount of necessary communication and improves the overall parallel efficiency of the implementation. The proposed AMR scheme was implemented using the message passing interface (MPI) library and the C++ programming language.[72]

As shown by Figure 2, ghost cells which surround the solution block and overlap cells on neighboring blocks are used to share solution content through inter-block communication. The conservation properties of the finite-volume discretization are retained across blocks with resolution changes by using the fine-grid interface flux to correct the flux computed on neighboring coarse blocks.[37,38] Passing these flux corrections and the overlapping cell solution content between processors at each stage of the integration scheme accounts for the main source of inter-processor communication.

VII. Results and Discussions

A. Fully-Developed Turbulent Pipe Flow

As partial validation of the numerical scheme and turbulence modelling, fully-developed turbulent pipe flow case was first considered. Numerical predictions were compared to the experimental data provided by Laufer[73] for a non-reacting, fully-developed turbulent pipe flow with Reynolds number of 50 000. Solutions for k-ω turbulence model with both direct integration to the wall and standard wall functions are compared to

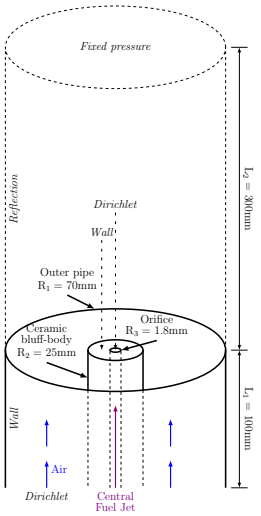

Figure 4: Schematic diagram of the Sydney bluff-body burner. The computational domain and boundary conditions used are also shown

measured mean axial velocity and turbulent kinetic energy in Figure 3. Calculations with the low-Reynolds-number formulation were performed using 64 cells in the radial direction with 3 to 4 of those cells lying within the laminar sublayer. The first cell off the wall was located at $y^+ \approx 0.6$. The results using the wall functions was obtained using 16 cells in the radial direction with the first cell located at $y^+ \approx 43$. Good agreement can be seen between the experimental data and the numerically predicted results. As expected, it is evident that the k-ω model is able to reproduce the characteristic features of fully-developed pipe flow.

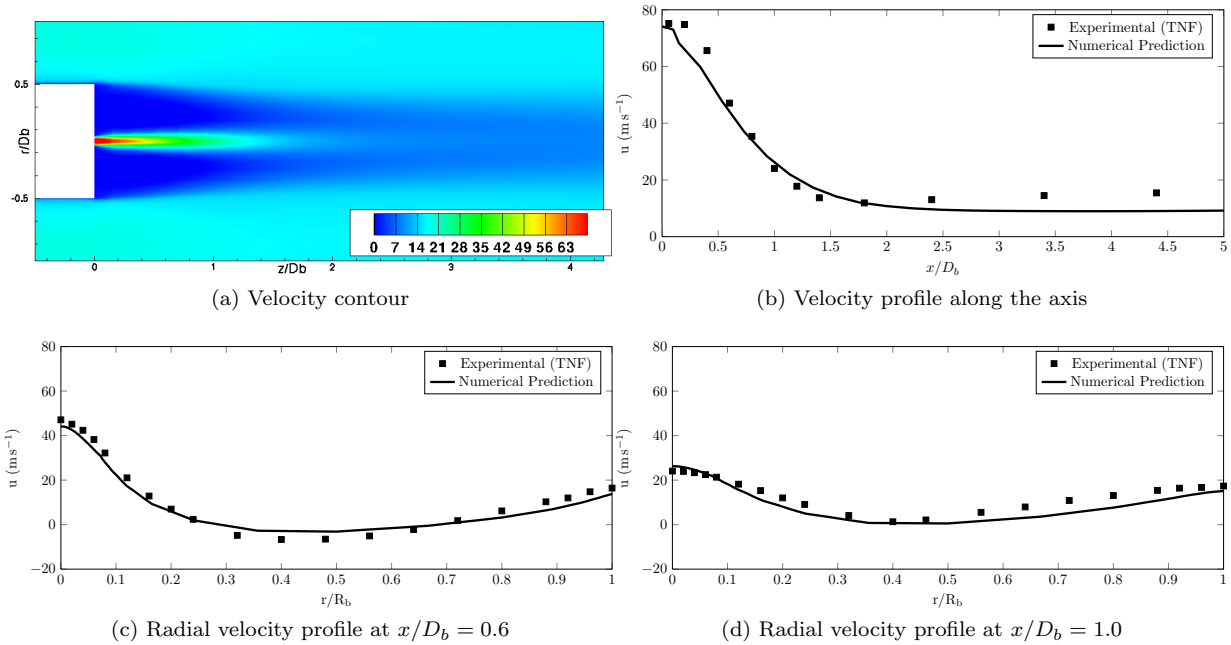

(a) Velocity contour

(b) Velocity profile along the axis

(c) Radial velocity profile at $x/D_b = 0.6$

(d) Radial velocity profile at $x/D_b = 1.0$

Figure 5: Comparison of predicted and measured velocity profiles of mean axial velocity at various locations downstream from the base of the bluff-body burner for non-reacting flow with air jet.

B. Bluff-body Burner

The Sydney bluff-body configuration, which forms part of the experimental database of the International Workshop on Measurement and Computation of Turbulent Non-premixed Flames (TNF),[74] has been con-

sidered in the present work. This burner has been investigated and/or used for verification and validation purposes in several recent studies by Masri *et al.*,[75–78] Dally *et al.*[79,80] and Gao and Groth.[48–50] A schematic diagram of the Sydney bluff-body burner configuration has been shown in Figure 4. The bluff-body has a radius $R_2 = 25\,\text{mm}$ and length $L_1 = 100\,\text{mm}$ and is located co-axially with the air flow inlet. The orifice at the center of the bluff-body has a radius $R_3 = 1.8\,\text{mm}$. The outer cylinder for air inflow has a radius of $R_1 = 70\,\text{mm}$. Adiabatic wall boundary conditions are used for the boundaries representing the bluff body. Dirichlet boundary conditions are used for the air inlet and the orifice. A reflection boundary condition is used at the outer boundary. The outlet of the flow domain, at a distance $L_2 = 300\,\text{mm}$ from the bluff body, has Neumann-type boundary conditions for all properties except pressure which is held constant.

1. *Non-Reacting Bluff-Body Burner Flow*

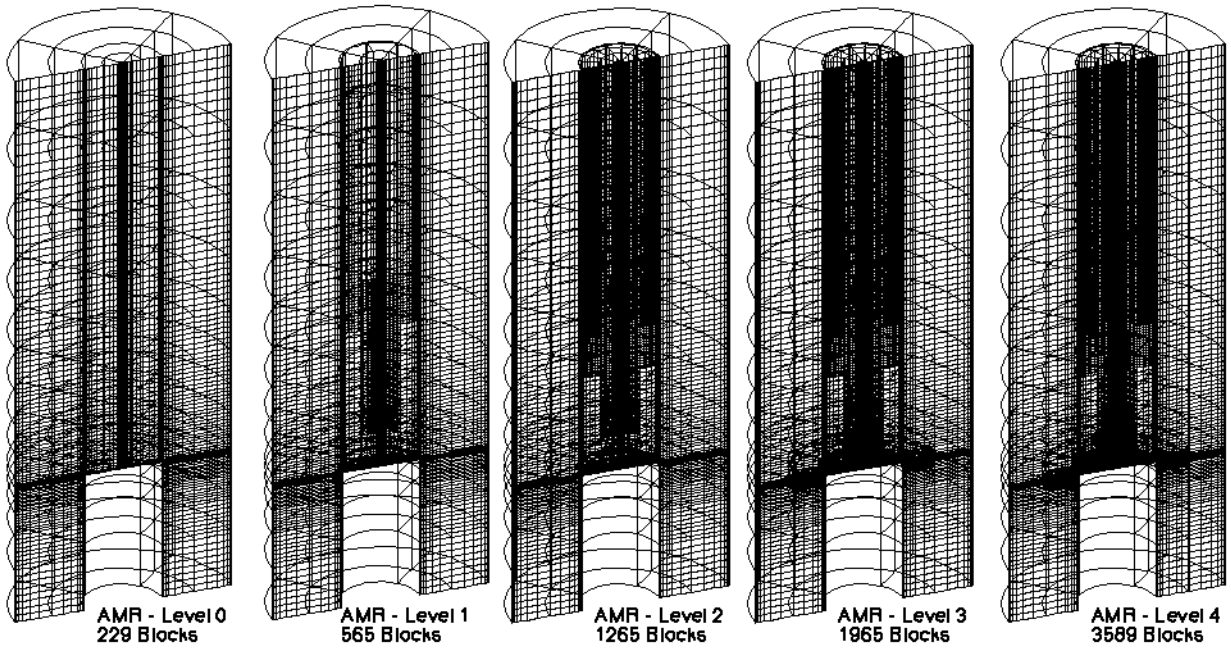

(a) The sliced three-dimensional grid after different levels of AMR refinement. Density gradient was chosen as the refinement criterion. Refinement can be seen at along the flame front where the maximum gradient exits. The grid shown is for the PCM-FPI Approach 1.

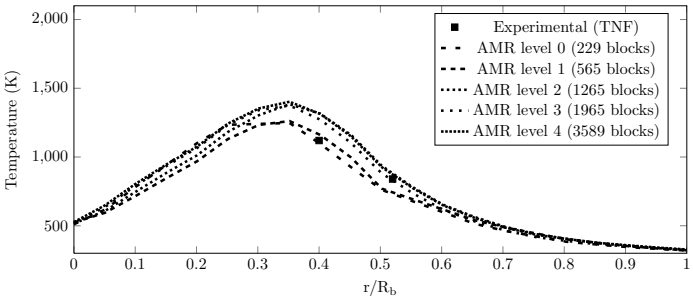

(b) Predicted temperature profiles at $x/D_b = 1.92$ downstream from the base of the bluff-burner burner after different levels of AMR refinement

Figure 6: AMR results using the proposed numerical scheme for fully three-dimensional flow geometries for bluff-body burner methane-air reacting flow.

The first bluff-body burner case considered is a non-reacting flow, where air is injected from both the fuel and the air inlet. Air is injected at the base of the bluff-body at 300 K with a parabolic profile having a mean velocity of 61 m/s. The mean velocity and temperature of the co-flow air are 20 m/s and 300 K respectively. The solution domain in initialized with a uniform solution state corresponding to quiescent air at 300 K.

EDM	PCM-FPI Approach 1	PCM-FPI Approach 2
4.4858 (1)	4.593 (1.024)	4.666 (1.04)

Table 2: The CPU time per iteration for different chemical kinetic mechanisms, using the present numerical scheme, for bluff-body burner methane-air reacting flow - the figures in bracket show the normalized value.

The Reynolds number and the Mach number of the high-speed jet are Re=193 000 and Ma=0.18. These flow conditions are classified as "jet-dominated", since the jet penetrates the re-circulation zone behind the wall of the bluff-body and propagates in a jet-like manner further downstream.

The non-reacting bluff-body burner flow was simulated using the proposed numerical scheme for three-dimensional flow geometries. The flow-field calculations were carried out on four adaptively refined grids, each consisting of a number of 8×8×8 cell blocks: 108 blocks (55 296 cells); 165 blocks (84 480 cells); 219 blocks (112 128 cells); and 388 blocks (198 656 cells). The velocity gradient was chosen as the refinement criterion. The threshold for refinement was chosen to be 0.5 and the threshold for coarsening was 0.1. The refinement efficiency of the AMR scheme after three levels of refinement was 0.968.

The agreement between the predictions and experiment is confirmed by a comparison of the predicted axial (centre-line) profile of the mean axial velocity component to the experimental results as depicted in Figure 5b. Also, the comparisons of the predicted radial profiles of the mean axial velocity to the measured data at two locations are shown in Figure 5c and Figure 5d. All of these figures show reasonably good agreement between the numerical results and the experimental data.

2. Reacting Bluff-Body Burner Flow

A three-dimensional turbulent diffusion flame for the Sydney bluff-body burner was also simulated using the proposed numerical scheme. In this case a methane gaseous fuel jet was injected at the base of the bluff-body with bulk velocity of 104 m/s at 300 K. The bulk velocity of co-flow air was 30 m/s. The Reynolds and Mach number of the methane jet are Re = 315 000 and Ma = 0.24.

The flow-field calculations were carried out on four adaptively refined grids, each consisting of a number of 8×8×8 cell blocks: 229 blocks (117 248 cells); 565 blocks (289 280 cells); 1265 blocks (647 680 cells); 1965 blocks (1 006 080 cells); and 3589 blocks (1 837 568 cells). These grids at different AMR levels for the reacting flow are shown in Figure 6a. Density gradient was chosen as the refinement criterion, with a threshold for refinement as 0.5 and the threshold for coarsening as 1.0. Block refinement can be seen along the flame front where the maximum density gradient exists. Figure 6 strongly demonstrates the capability of the AMR algorithm to refine the grid in regions of maximum physical activity. Figure 6b shows the radial profile of temperature at $x/D_b = 1.92$ downstream from the base of the burner for different levels of AMR. It can be seen that after two levels of AMR, a grid converged solution was obtained. An AMR refinement efficiency of 0.996 was obtained after four levels of refinement. Figure 6 strongly demonstrates the capability of the AMR algorithm to refine the grid in regions of maximum physical activity.

Figure 7 compares the predicted distribution of temperature and some species in the solution domain. The maximum temperature predicted by the PCM-FPI approach is almost 500 K lower than the temperature predicted by the EDM scheme. It is also more closer to the recorded maximum experimental data of 1200 K. Figure 8 shows the solution profiles obtained using the different numerical approaches to treat chemistry. Figure 8a shows that the temperature profiles are in far better agreement with the experimental data, in comparison to the EDM result. In Figure 8b the EDM passes through the experimental points considerably closely than the PCM-FPI lines do. However, the variation between the maximum CO_2 predicted by EDM and that of the experimental data is much higher in comparison to the PCM-FPI results. Apart from this, the PCM-FPI approach also gives predictions for the minor species like OH, CO, and, C_2H_2, as shown in Figure 7c and Figure 7d, which is not possible to obtain using the EDM approach.

It is noted above that the temperature is somewhat over-predicted by the proposed parallel AMR scheme for this case. It maybe because of neglecting the radiation transport in the simulation. Note that while radiation effects may influence the predicted temperature for this case, Merci *et al.*[81,82] argue that, since the flame is unconfined and very little soot is formed, radiation effects should be relatively small. Some other reasons might be the use of β-distribution for averaging the tabulated quantities. It would be of interest to see the temperature predictions by using other averaging procedures with the tabulated-chemistry approach.

Table 2 compares the computational cost of each chemical-kinetic scheme. The cost of the PCM-FPI scheme is only marginally higher than the EDM methods. This result is very encouraging as it shows that by using the PCM-FPI approach detail-chemistry results can be obtained without much computational overhead in comparison to the EDM scheme. This can be attributed to the fact that the computational cost involved in reconstruction for the three-dimensional geometry is quite expensive. The additional computational cost associated with the PCM-FPI Approaches is insignificant compared to the cost involved for three-dimensional FVM. Hence, when used with the numerical scheme for three-dimensional geometry, the computational cost remains practically unaffected.

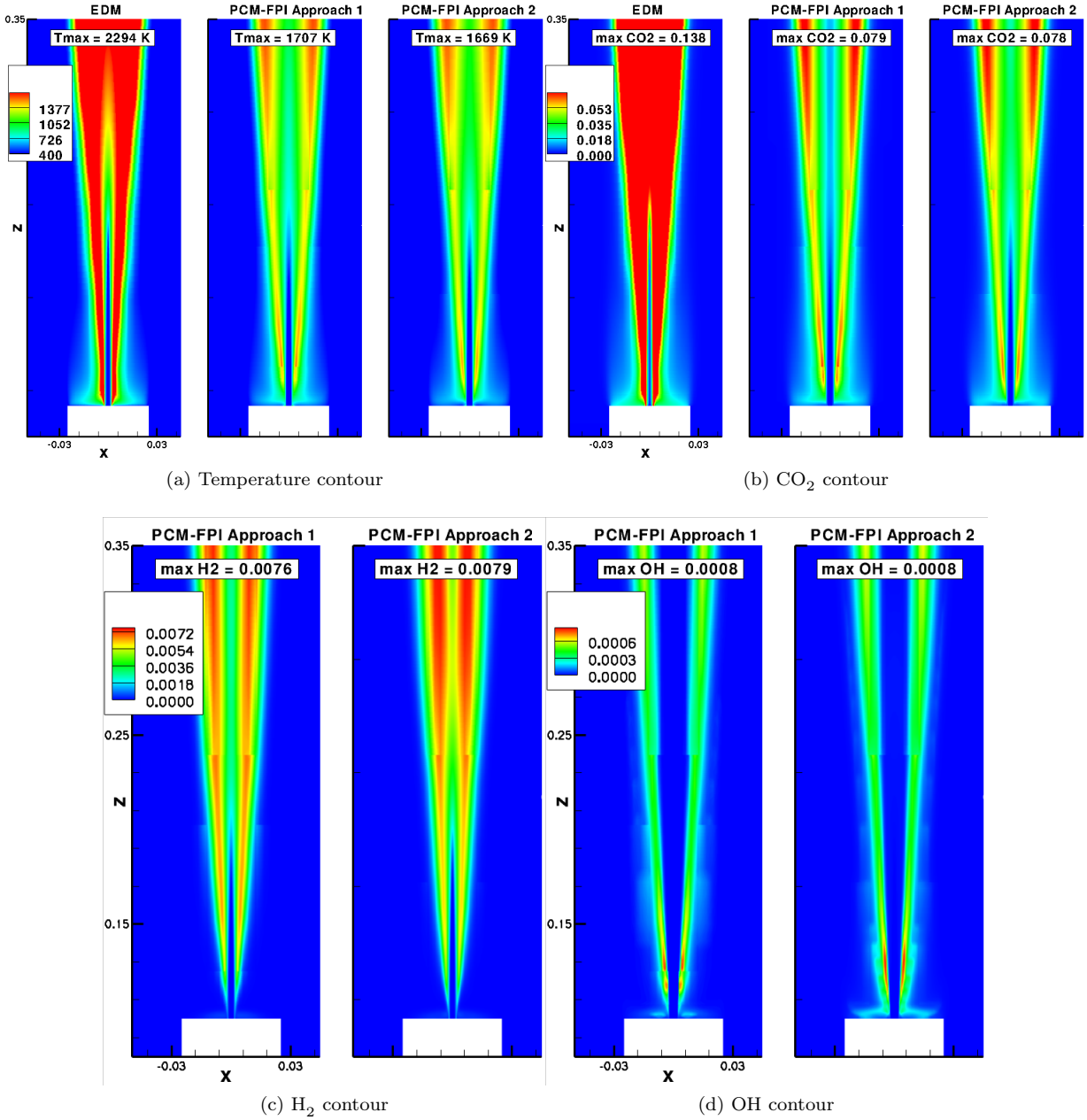

(a) Temperature contour

(b) CO_2 contour

(c) H_2 contour

(d) OH contour

Figure 7: The solution contours predicted for different chemical kinetic mechanisms, using the present numerical scheme, for methane-air diffusion flame.

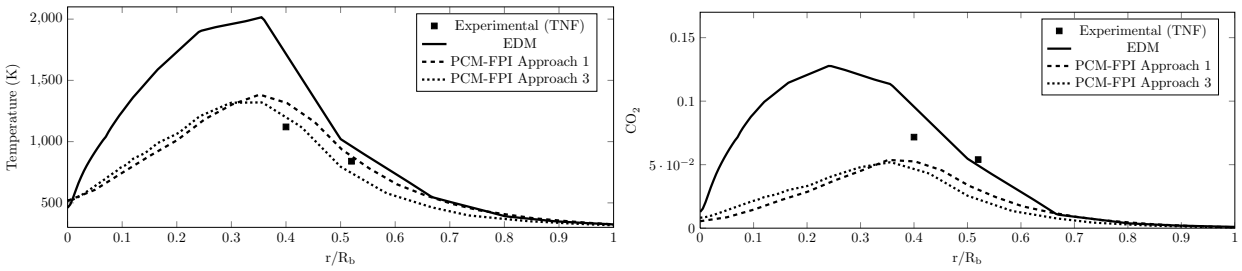

(a) Radial profile of mean Temperature

(b) Radial profile of mean mass fraction of CO_2

Figure 8: Comparison of predicted profiles and measured data at $x/D_b = 1.92$ downstream from the base of the bluff-burner burner using the present numerical scheme for reacting flow with methane jet.

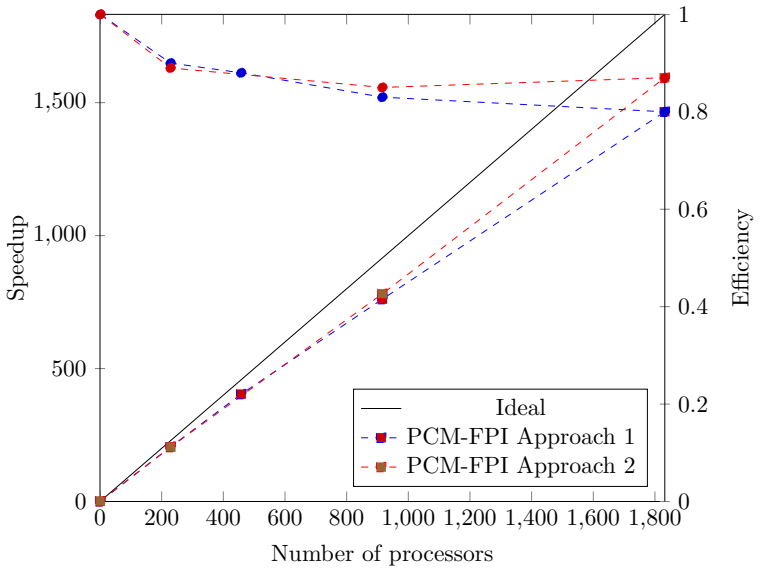

Figure 9: Parallel performance of the proposed solution algorithm showing the strong scaling for PCM-FPI Approach 1 and PCM-FPI Approach 2 for the methane-air turbulent diffusion flame simulations.

C. Parallel performance

The parallel performance of the proposed algorithm was assessed for strong scaling as part of this research. Strong scaling is a measure of the ability to demonstrate a proportionate increase in parallel speedup with more processors. For a strong scaling test, the problem size is generally held fixed while the number of processors used to perform the computation is varied. Scaling is measured by the parallel speedup, S_p, and efficiency, η_p, which are then defined as

$$S_p = \frac{t_1}{t_p} \tag{53}$$

$$\eta_p = \frac{S_p}{p} \tag{54}$$

where t_p is the total wall times required to solve the problem with p processors.

Strong scaling of both PCM-FPI tabulated approaches were examined. For both approaches, the strong scaling test was carried out using a grid which consisted of 1832 grid blocks. These grids were obtained after one level of uniform AMR refinement on the initial grid of 229 blocks. The work load per processor was varied without affecting the partitioning of the mesh by changing the number of blocks assigned to each processor. As a result, only the effect of inter-processor communication on parallel efficiency was taken into account.

The resulting relationship between parallel speedup, efficiency, and number of processors is shown in Figure 9 for the methane-air turbulent diffusion flame Sydney bluff-body configuration. Excellent parallel performance is achieved with an efficiency of 80 % and 87 % for PCM-FPI Approach 1 and PCM-FPI Approach 2, respectively, for up to 1832 processors. These results clearly show that the proposed PCM-FPI algorithm scales extremely well within the parallel AMR solution scheme.

VIII. Conclusion

A new parallel adaptive mesh refinement based finite-volume scheme was presented to model detailed-chemistry effects on turbulent diffusion flames using the PCM-FPI approach. The Sydney bluff-body burner was used as the validation case and the predicted results were compared to the experimental as well as the simplified one-step EDM chemical kinetic scheme. Much better agreement was seen between the experimental and the PCM-FPI results than the EDM predictions. Moreover, the PCM-FPI scheme was only marginally more expensive than the EDM model in terms of computational costs involved. The parallel performance of the PCM-FPI scheme was investigated on a large parallel distributed-memory multi-processor cluster. It was found that the algorithm scales extremely well with an efficiency of more than 80% for around 1850 processors. The AMR capability of the algorithm was also examined for the three-dimensional grid used for the Sydney bluff-body burner. Maximum grid refinement was seen in regions with highest value of temperature gradient, which demonstrated the solution-adaptivity of the AMR scheme. A refinement efficiency of around 0.996 was achieved after four levels of refinement.

Acknowledgments

Computational resources for performing the calculations reported herein were provided by the SciNet High Performance Computing Consortium at the University of Toronto and Compute/Calcul Canada through funding from the Canada Foundation for Innovation (CFI) and the Province of Ontario, Canada.

References

[1]Smith, G. P., Golden, D. M., Frenklach, M., Moriarty, N. W., Eiteneer, B., Goldenberg, M., Bowman, C. T., Hanson, R. K., Song, S., Gardiner, W. C., Lissianski, V. V., and Qin, Z., "GRI-Mech 3.0," http://www.me.berkeley.edu/gri_mech/.

[2]Turns, S. R., editor, *An Introduction to Combustion*, McGraw-Hill, New York, 2000.

[3]Curran, H. J., Gaffuri, P., Pitz, W. J., and Westbrook, C. K., "A Comprehensive Modeling Study of iso-Octane Oxidation," *Combustion and Flame*, Vol. 129, No. 3, 2002, pp. 253–280.

[4]Lindstedt, R. P. and Maurice, L. Q., "Detailed Chemical-Kinetic Model for Aviation Fuels," *J. Plasma Physics*, Vol. 16, 2000, pp. 187–195.

[5]Maas, U. and Pope, S. B., "Simplifying Chemical Kinetics: Intrinsic Low-Dimensional Manifolds in Composition Space," *Combustion and Flame*, 1992, pp. 239–264.

[6]Peters, N., "Reducing Mechanisms," 1991.

[7]Lam, S. H. and Goussis, D. A., "Conventional Asymptotics and Computational Singular Perturbation for Simplified Kinetics Modeling," 1991.

[8]Tonse, S. R., Moriarty, N. W., Frenklach, M., and Brown, N. J., "Computational economy improvements in PRISM," *International Journal of Chemical Kinetics*, Vol. 35, No. 9, 2003, pp. 237–253.

[9]Ren, Z. and Pope, S. B., "Entropy Production and element conservation in the quasi-steady-state approximation," *Combustion and Flame*, Vol. 137, 2004, pp. 251–254.

[10]Bykov, V. and Maas, U., "The extension of ILDM concept to reaction-diffusion manifolds," *AIAA J.*, Vol. 11, No. 6, 2007, pp. 839–862.

[11]Ren, Z. and Pope, S. B., "Reduced Description of Complex Dynamics in Reactive Systems," *Journal of Physical Chemistry*, Vol. 111, 2007, pp. 8464–8474.

[12]Peters, N., "Laminar Diffusion Flamelet Models in Non-Premixed Turbulent Combustion," *Prog. Energy Combustion Sci.*, Vol. 10, 1984, pp. 319–339.

[13]Bradley, D. and Lau, A. K. C., "The Mathematical Modelling of premixed turbulent combustion," *Pure and Applied Chemistry*, Vol. 62, 1990, pp. 803–814.

[14]Bradley, D., Kwa, L. K., Lau, A. K. C., Missaghi, M., and Chin, S. B., "Laminar flamelet modeling of recirculating premixed methane and propane-air combustion," *Combustion and Flame*, Vol. 71, 1988, pp. 109–122.

[15]Gicquel, O., Darabiha, N., and Thévenin, D., "Laminar premixed hyrogen/air counterflow flame simulations using flame prolongation of ILDM with differential diffusion," *Proceedings of the Combustion Institute*, Vol. 28, 2000, pp. 1901–1908.

[16]Fiorina, B., Gicquel, O., Vervisch, L., Carpentier, S., and Darabiha, N., "Premixed turbulent combustion modeling using tabulated detailed chemistry and PDF," *Proceedings of the Combustion Institute*, Vol. 30, 2005, pp. 867–874.

[17]van Oijen, J. A. and de Goey, L. P. H., "Modeling of Premixed Laminar Flames using Flamelet-Generated Manifolds," *Combustion Science and Technology*, Vol. 161, 2000, pp. 113–137.

[18]Ribert, G., Champion, M., Gicquel, O., Darabiha, N., and Veynante, D., "Modeling nonadiabatic turbulent premixed reactive flows including tabulated chemistry," *Combustion and Flame*, Vol. 141, May 2005, pp. 271–280.

[19]Domingo, P., Vervisch, L., and Sandra Payet, R. H., "DNS of a premixed turbulent V flame and LES of a ducted flame

using a FSD-PDF subgrid scale closure with FPI-tabulated chemistry," *Combustion and Flame*, 2005, pp. 566–586.
[20]Fiorina, B., Gicquel, O., Vervisch, L., Carpentier, S., and Darabiha, N., "Approximating the chemical structure of partially premixed and diffusion counterflow flames using FPI flamelet tabulation," *Combustion and Flame*, Vol. 140, 2005, pp. 147–160.
[21]Vervisch, L., Hauguel, R., Domingo, P., and Rullaud, M., "Three facets of turbulent combustion modelling: DNS of premixed V-flame, LES of lifted nonpremixed flame and RANS of jet-flame," *Journal of Turbulence*, Vol. 4, 2004, pp. 1–36.
[22]Bradley, D., Gaskell, P. H., and Gu, X. J., "The Mathematical Modeling of Liftoff and Blowoff of Turbulent Non-premixed Methane Jet Flames At High Strain Rates," *Twenty Seventh Symposium (International) on Combustion*, Vol. 27, 1998, pp. 1199–1206.
[23]Chen, J.-Y. and Dibble, W. K. R. W., "PDF modeling of Turbulent Nonpremixed Methane Jet Flames," *Combustion Science and Technology*, Vol. 64, No. 4, 1989, pp. 315–346.
[24]Norris, A. T. and Pope, S. B., "Modeling of Extinction in Turbulent Diffusion Flames by the Velocity-Dissipation-Composition PDF Method," *Combustion and Flame*, Vol. 100, 1995, pp. 211–220.
[25]Saxena, V. and Pope, S. B., "PDF Simulations of Turbulent Combustion Incorporating Detailed Chemistry," *Combustion and Flame*, Vol. 117, 1999, pp. 340–350.
[26]Domingo, P., Vervisch, L., and Veynante, D., "Large-Eddy simulation of a lifted methane jet flame in a vitiated coflow," *Combustion and Flame*, Vol. 152, 2008, pp. 415–432.
[27]Richardson, J. M., Howard, H. C., and Smith, R. W., 1953, p. 814.
[28]Spalding, D. B., "Concerning Fluctuations in a Round Turbulent Free Jet," *Chemical Engineering Science*, Vol. 26, January 1971, pp. 95–107.
[29]Lockwood, F. C. and Naguib, A. S., "The Prediction of Fluctuations in the Properties of Free, Round-Jet, Turbulent, Diffusion Flames," *Combustion and Flame*, Vol. 24, 1975, pp. 109–124.
[30]Rhodes, R. P. and Harsha, A. P. T., "On Putting the 'Turbulence' in Turbulent Reacting Flows," Paper 72-68, AIAA, 1972.
[31]Jones, W. P., "Models for turbulent flows with variable density and combustion," *von Karman Institute for Fluid Dynamics Lecture Series 1979-2, Prediction Methods for Turblent Flows*, edited by W. Kollmann, Hemisphere Publication Corp., Washington, 1980.
[32]Libby, P. A. and Williams, F. A., *Turbulent flows with nonpremixed reactants*, Springer-Verlag, Berlin, 1980.
[33]Kent, H. J. and Bilger, R. W., "Turbulent Diffusion Flames," *Fourteenth International Symposium on Combustion*, 1973, p. 615.
[34]Godel, G., Domingo, P., and Vervisch, L., "Tabulation of NOx chemistry in Large-Eddy Simulation of non-premixed turbulent flames," *Proceedings of the Combustion Institute*, Vol. 32, 2009, pp. 1555–1561.
[35]Subramanian, V., Domingo, P., and Vervisch, L., "Large eddy simulation of forced ignition of an annular bluff-body burner," *Combustion and Flame*, Vol. 157, 2010, pp. 579–601.
[36]Hernàndez-Pérez, F. E., Yuen, F., Groth, C., and Ö.L.Gulder, "LES of a laboratory-scale turbulent premixed Bunsen flame using FSD, PCM-FPI and thickened flame models," accepted in the Proceedings of the Combustion Institute, doi:10.1016/j.proci.2010.06.010., 2010.
[37]Berger, M. J., "Adaptive Mesh Refinement for Hyperbolic Partial Differential Equations," *J. Comput. Phys.*, Vol. 53, 1984, pp. 484–512.
[38]Berger, M. J. and Colella, P., "Local Adaptive Mesh Refinement for Shock Hydrodynamics," *J. Comput. Phys.*, Vol. 82, 1989, pp. 67–84.
[39]Quirk, J. J., *An Adaptive Grid Algorithm for Computational Shock Hydrodynamics*, Ph.D. thesis, Cranfield Institute of Technology, January 1991.
[40]De Zeeuw, D. and Powell, K. G., "An Adaptively Refined Cartesian Mesh Solver for the Euler Equations," *J. Comput. Phys.*, Vol. 104, 1993, pp. 56–68.
[41]Quirk, J. J. and Hanebutte, U. R., "A Parallel Adaptive Mesh Refinement Algorithm," Report 93-63, ICASE, August 1993.
[42]Aftosmis, M. J., Berger, M. J., and Melton, J. E., "Robust and Efficient Cartesian Mesh Generation for Component-Base Geometry," *AIAA J.*, Vol. 36, No. 6, 1998, pp. 952–960.
[43]Groth, C. P. T., Zeeuw, D. L. D., Powell, K. G., Gombosi, T. I., and Stout, Q. F., "A Parallel Solution-Adaptive Scheme for Ideal Magnetohydrodynamics," Paper 99-3273, AIAA, June 1999.
[44]Groth, C. P. T., De Zeeuw, D. L., Gombosi, T. I., and Powell, K. G., "Global Three-Dimensional MHD Simulation of a Space Weather Event: CME Formation, Interplanetary Propagation, and and Interaction with the Magnetosphere," *J. Geophys. Res.*, Vol. 105, No. A11, 2000, pp. 25,053–25,078.
[45]Day, M. S. and Bell, J. B., "Numerical Simulation of Laminar Reacting Flows with Complex Chemistry," *Combust. Theory Modelling*, Vol. 4, No. 4, 2000, pp. 535–556.
[46]Bell, J., Day, M., Almgren, A., Lijewski, M. J., and Rendleman, C. A., "Adaptive Numerical Simulation of Turbulent Premixed Combustion," *Proceedings of the First MIT Conference on Computational Fluid and Solid Mechanics*, June 2001, p. 1.
[47]Bell, J., Day, M., Almgren, A., Lijewski, M. J., and Rendleman, C. A., "A Parallel Adaptive Projection Method for Low Mach Number Flows," *Int. J. Numer. Meth. Fluids*, Vol. 40, 2002, pp. 209–216.
[48]Gao, X. and Groth, C. P. T., "A Parallel Adaptive Mesh Refinement Algorithm for Predicting Turbulent Non-Premixed Combusting Flows," *Int. J. Comput. Fluid Dyn.*, Vol. 20, No. 5, 2006, pp. 349–357.
[49]Gao, X. and Groth, C. P. T., "Parallel Adaptive Mesh Refinement Scheme for Three-Dimensional Turbulent Non-Premixed Combustion," Paper 2008-1017, AIAA, January 2008.
[50]Gao, X. and Groth, C. P. T., "A Parallel Solution-Adaptive Method for Three-Dimensional Turbulent Non-Premixed Combusting Flows," *J. Comput. Phys.*, Vol. 229, No. 5, 2010, pp. 3250–3275.
[51]Kuo, K., *Principles of Combustion*, John Wiley & Sons, 1986.
[52]Aris, R., *Vectors, Tensors and the Basic Equations of Fluid Mechanics*, Dover Publications, New Jersey, 1989.
[53]Wilcox, D., *Turbulence Modeling for CFD*, DCW Industries, 2002.
[54]Gordon, S. and McBride, B. J., "Computer Program for Calculation of Complex Chemical Equilibrium Compositions and Applications I. Analysis," Reference Publication 1311, NASA, 1994.
[55]McBride, B. J. and Gordon, S., "Computer Program for Calculation of Complex Chemical Equilibrium Compositions and Applications II. Users Manual and Program Description," Reference Publication 1311, NASA, 1996.

[56]Gao, X. and Groth, C. P. T., "Parallel Adaptive Mesh Refinement Scheme for Turbulent Non-Premixed Combusting Flow Prediction," Paper 2006-1448, AIAA, January 2006.
[57]Goodwin, D. and Moffat, H. K., "Cantera," http://code.google.com/p/cantera/.
[58]Fiorina, B., Baron, R., Gicquel, O., Vervisch, L., Carpentier, S., and Darabiha, N., "Modelling non-adiabatic partially premixed flames using flame-prolongation of ILDM," *Combustion Theory and Modelling*, Vol. 7, 2003, pp. 449–470.
[59]Jha, P. K. and Groth, C. P. T., "Evaluation of Flame-Prolongation of ILDM and Flamelet Tabulated Chemistry Approaches for Laminar Flames," Paper, AIAA, January 2011.
[60]Galpin, J., *Modélisation LES de la combustion avec une prise en compte des effets de cinétique détaillée et en perspective d'application moteur*, Ph.D. thesis, IFP, Division Techniques d'Applications Énergétiques, September 2007.
[61]Galpin, J., Naudin, A., Vervich, L., Angelberger, C., Colin, O., and Domingo, P., "Large-eddy simulation of a fuel-lean premixed turbulent swirl-burner," *Combustion and Flame*, Vol. 155, 2008, pp. 247–266.
[62]Matthieu, R., *Modélisation de la combustion turbulente via une méthode de tabulation de la cinétique chimique détaillée couplée à des fonctions densités de probabilité Application aux foyers aéronautiques*, Ph.D. thesis, L'INSA De ROUEN, June 2004.
[63]Barlow, R. S. and Frank, J. H., "Effects of turbulence on species mass fractions in methane/air jet flames," *Twenty-Seventh Symposium (International) on Combustion*, The Combustion Institute, Pittsburgh, 1998, pp. 1087–1095.
[64]Libby, P. and Williams, F. A., editors, *Turbulent reacting flows*, chap. 4, Academic Press Inc., 1994.
[65]Bray, K. N. C., "The Challenge of Turbulent Combustion," Paper, Twenty-Sixth Symposium (International) on Combustion/The Combustion Institute, 1996.
[66]Magnussen, B. and Hjertager, B., "On mathematical modeling of turbulent combustion with special emphasis on soot formation and combustion," *Sixteenth Symposium (International) on Combustion*, The Combustion Institute, 1976, pp. 719–729.
[67]Westbrook, C. K. and Dryer, F. L., "Simplified Reaction Mechanisms for the Oxidation of Hydrocarbon Fuels in Flames," *Combust. Sci. Tech.*, Vol. 27, 1981, pp. 31–43.
[68]Barth, T. J., "Recent Developments in High Order K-Exact Reconstruction on Unstructured Meshes," Paper 93-0668, AIAA, January 1993.
[69]Liou, M.-S., "A Sequel to AUSM, Part II: AUSM$^+$-up for all speeds," *J. Comput. Phys.*, Vol. 214, 2006, pp. 137–170.
[70]Coirier, W. J. and Powell, K. G., "Solution-Adaptive Cartesian Cell Approach for Viscous and Inviscid Flows," *AIAA J.*, Vol. 34, No. 5, May 1996, pp. 938–945.
[71]Berger, M. J. and Saltzman, J. S., "AMR on the CM-2," *Appl. Numer. Math.*, Vol. 14, 1994, pp. 239–253.
[72]Gropp, W., Lusk, E., and Skjellum, A., *Using MPI*, MIT Press, Cambridge, Massachussets, 1999.
[73]J.Laufer, "The Structure of Turbulence in Fully Developed Pipe Flow," Report 1174, NACA, 1954.
[74]"International Workshop on Measurement and Computation of Turbulent Nonpremixed Flames," http://www.ca.sandia.gov/TNF/.
[75]Masri, A. R., Dibble, R. W., and Barlow, R. S., "The Structure of Turbulent Nonpremixed Flames of Methanol over a Range of Mixing Rates," *Combustion and Flame*, Vol. 89, 1992, pp. 167–185.
[76]Masri, A. R., Dibble, R. W., and Barlow, R. S., "Raman-Rayleigh Measurements in Bluff Body Stabilised Flames of Hydrocarbon Fuels," *Twenty-fourth Symposium (International) on Combustion*, The Combustion Institute, 1992, pp. 317–324.
[77]Masri, A. R., Dally, B. B., and Barlow, R. S., "The Structure of the Recirculation Zone of a Bluff-Body Combustor," *Twenty-fifth Symposium (International) on Combustion*, The Combustion Institute, 1994, pp. 1301–1308.
[78]Masri, A. R., Kelman, J. B., and Dally, B. B., "The Instantaneous Spatial Structure of the Recirculation Zone in Bluff-Body Stabilised Flames," *Proceedings of the Combustion Institute*, The Combustion Institute, 1998, pp. 1031–1038.
[79]Dally, B. B., Fletcher, D. F., and Masri, A. R., "Modelling of Turbulent Flames Stabilised on a Bluff-Body," *Combust. Theory Modelling*, Vol. 2, 1998, pp. 193–219.
[80]Dally, B. B., Masri, A. R., Barlow, R. S., and Fiechtner, G. J., "Instantaneous and Mean Compositional Structure of Bluff-Body Stabilised Nonpremixed Flames," *Combust. Theory Modelling*, Vol. 114, 1998, pp. 119–148.
[81]Merci, B., *An Unstructured Parallel Algorithm for Large Eddy and Conjugate Heat Transfer Simulations*, Ph.D. thesis, Ghent University, 2000.
[82]Merci, B., Dick, E., Vierendeels, J., Roekaerts, D., and Peeters, T. W. J., "Application of a New Cubic Turbulence Model to Piloted and Bluff-Body Diffusion Flames," *Combustion and Flame*, Vol. 126, No. 1-2, 2001, pp. 1533–1556.